



POWDER-BASED FUNCTIONAL MATERIALS FOR EXTREME ENVIRONMENTS: PROCESSING AND CHARACTERIZATION

Production of AA 2014 Matrix Wollastanite/Wood Ash Solid Waste Particle Reinforced Hybrid Composite with Powder Metallurgy and Investigation of Its Structural Properties

HAKAN GÖKMEŞE ^{1,2} and ŞABAN BÜLBÜL¹

1.—Department of Mechanical Engineering, Ahmet Cengiz Engineering Faculty, Necmettin Erbakan University, 42360 Konya, Turkey. 2.—e-mail: hakan1440@gmail.com

In this study, using AA 2014 aluminum alloy, AA2014/wollastanite, AA2014/wood ash, and AA2014/wollastanite/wood ash composite hybrid materials were produced by powder metallurgy method. The powders, whose mixing ratios were determined by weight, were mixed in a 3-dimensional mixer for 30 min. The prepared mixture powders were pressed uniformly under a pressure of 700 MPa, and cylindrical materials with a diameter of 10 mm were obtained. Then, the materials were sintered for 1 h under argon gas flow at a temperature of 600°C. The density, microstructure, hardness, and wear behavior of the materials were examined. It was observed that the density of the composite materials increased relatively compared to AA 2014 alloy. As the particle reinforcement ratios increased, porosity amounts also increased in the composite and especially in the hybrid materials. In the wood ash-reinforced composite materials, the particles were distributed more homogeneously in the microstructure. The highest hardness value obtained was 70.65 HV in AA2014/15% wollastanite composite material. The weight loss increased in the materials created by particle reinforcement, and the lowest weight loss (170 mg) was determined in this material.

INTRODUCTION

The need for composite materials has become a necessity for modern technology due to advanced physical and mechanical properties. Metal matrix composites (MMCs) have been developed in recent years, and aluminum matrix composites (AMCs), which are among them, have started to be used in many areas of industry. The main reason for this is that their densities are low, while their toughness and corrosion resistance are high.^{1–3} The powder metallurgy (PM) method mean we can obtain superior properties that cannot be obtained from single-material-produced composite materials by combining two materials, one of which is of ceramic origin and the other is metal, which cannot be combined with any other production method. Different matrix–reinforcement combinations can be used in

MMC systems. Among matrix materials, pure aluminum and aluminum alloys, especially AA 2014 aluminum alloy, constitute the most preferred material group with their low density, high strength, toughness, corrosion resistance, and easy machinability.⁴ The most common types of ceramic particles added to the aluminum matrix to form composite materials include Al_2O_3 , SiC, and B_4C , and these ceramic particles added to the matrix structure (AA 2014) and aluminum have played an important role in the development of MMCs.⁵ Hybrid metal matrix composites are advanced technological engineering materials created by using two or more reinforcement elements together.⁶ The main reason why hybrid composite materials are included in the class of materials mainly used in the aerospace industry is that they have superior mechanical and physical properties.⁷ However, the use of industrial materials, such as Al_2O_3 , SiC, and B_4C , as reinforcement materials has pushed scientists to research different sources, because they increase production costs and are not

(Received May 21, 2023; accepted January 2, 2024; published online January 25, 2024)

environmentally friendly. In other respects, the disposal of agricultural wastes by burning causes great environmental pollution. Considering all the factors, scientists have turned to agricultural waste-based supplements due to their cost, applicability, and abundance, and they have investigated the usability of these wastes in MMCs and their results.^{8,9} Many of these researches are related to the investigation and reporting of MMCs obtained by using agricultural waste (naturally reinforced particles). When the literature is examined, it is seen that there are many studies where agricultural waste is used as a reinforcing material in AMC materials. The development of environmental awareness, the conversion of waste into products with higher added value, and the availability of agricultural waste and its cheap cost have played an important role in the use of these wastes as reinforcement materials in AMCs.¹⁰ In many studies, it has been reported that agricultural-reinforced composites are softer and more ductile than ceramic-reinforced composites and do not have a brittle structure.¹¹ Based on all these data, it is possible to say that, instead of costly and environmentally harmful ceramic-reinforced AMCs used in various automotive and aerospace applications, it would be preferable to use AMCs which are reinforced with lower-cost agricultural waste and have a high strength-to-weight ratio. Scientists have shown that many agricultural wastes, such as rice husk (paddy), peanut husk, corn cob ash, palm leaf, bamboo leaf ash, and aloe vera powder, can be used as reinforcement materials for aluminum metal matrix composites.^{12–16} In their study, Abdulrazaq et al. examined the morphological and solid phase properties of AMC samples produced by adding agricultural waste (palm kernel ash) at a rate of 2.5 wt.%, 5 wt.%, 7.5 wt.%, and 10 wt.% in addition to the aluminum matrix. In their experimental study, they reported that there was an increase in the hardness and compressive strength of palm kernel-added AMCs, and a decrease in their density.¹⁷ In other studies, scientists have emphasized that rice husk ash reinforced in AMCs improves mechanical properties.^{18–20} In another study, Satheesh and colleagues added 10 wt.% silicon carbide to an aluminum alloy, as well as coconut shell ash in proportions ranging from 2 wt.% to 10 wt.%. They investigated the optimum tensile strength and hardness of the AMC material they produced and revealed that the hardness and strength were obtained from a composite material in which coconut shell ash particles were used at a rate of 8 wt.%. They reported that the fact that coconut shell ash was more than 8 wt.% caused a decrease in tensile strength and hardness.²¹ In other studies where coconut shell ash has been used as a reinforcing material in AMCs, it has been stated that it improves the combustion temperature and mechanical properties.^{22–24}

In this study, wood ash and wollastonite, which are considered agricultural waste, were used as reinforcement materials in different proportions instead of the traditional ceramic materials in AA2014 matrix materials. When the production methods in which agricultural waste is used as reinforcement are examined, it is seen that many of them are produced by the casting method. In this study, for the first time, AMCs were produced by the powder metallurgy method by using wood ash as a reinforcement element. Thus, this study will be an indication that AMCs can be produced using agricultural wastes not only by the casting method but also by the powder metallurgy method.

MATERIALS AND METHODS

AA2014 pre-alloyed aluminum powders (Nanography Nano Technology, Turkey) were used as the main matrix in this study. The matrix material and the chemical compositions of CaSiO₃ (Izoref Industrial Products, Turkey) and wood ash (Kafkas Etlikmek, Turkey) used as particle reinforcement in the production of metal matrix ceramic-reinforced composite materials are given in Table I. The density and particle sizes of the matrix and reinforcement particles used in the experimental studies were AA 2014 alloy (2.80 g/cm³, < 100 μm), wollastonite (2.90 g/cm³, < 10 μm), and wood ash (2.50 g/cm³, < 5 μm).

AA2014 aluminum powders were used as the metal matrix, and CaSiO₃ and wood ash were used as additional ceramic phase particle reinforcement. The mixing rates were first determined in the production of the composite and hybrid materials, then, the AA 2014 alloy powder without reinforcement was prepared. Following this, the composite and hybrid experimental sample powder mixtures were prepared by adding CaSiO₃, wood ash, and CaSiO₃–wood ash in the proportions of 5%, 10%, and 15% to the AA2014 aluminum matrix alloy powder, respectively. The powder mixtures, weighed with Precisa precision scales, were transferred to a plastic container and mixed for 30 min with a 3-dimensional Turbula mixer (Turbulo-Wab, USA). After the mixing process, the powders were put into a mold and pressed uniformly under 700-MPa pressure in a 60-ton hydraulic press (Hidrolik-san, Turkey). They were then sintered at a temperature of 600°C for 1 h. Using argon gas in the medium during sintering, swept out the oxygen from the medium and prevented the oxidation of the experimental samples. The experimental samples produced were coded into three different groups (as WO5, WO10, and WO15, W5, W10, and W15, and, for hybrid composite material, H5, H10, and H15) based on the non-reinforced AA 2014 alloy and the increased wollastonite and wood ash contents. In order to prevent the samples from oxidation, they were kept in a vacuum desiccator atmosphere. The density results were calculated by making three

Table I. Chemical compositions of matrix and reinforcement powders (%)

Element	Al	Cu	Si	Mn	Mg	Fe	Zn	Cr	Ti	
AA 2014										
Rate (wt.%)	Balance	1.2–1	0.4	0.3	2.1–2.9	0.5	5.1–5.6	0.18–0.28	0.2	
Element	CaO		SiO ₂		Al ₂ O ₃		Fe ₂ O ₃			
Wollastonite										
Rate (wt.%)	48.48		48.52		0.24		0.26			
Element	Ca	K	Mg	S	P	Mn	Zn	Fe	Al	Na
Wood ash										
Rate (wt.%)	31.35	10.25	7.57	1.21	0.56	0.14	0.08	0.09	0.03	0.06

repetitive measurements for each sample and taking the arithmetic average. The density measurements for each of the experimental samples were calculated on a Precisa precision scale by applying the Archimedes principle. The formula used in the calculations was:

$$d = \frac{m}{V_y - V_s} \quad (1)$$

where d = density (g/cm^3), m = weight (g), V_y = wet weight (g), and V_s = weight in water (g).

In order to characterize the microstructures of composite materials, the surfaces of the samples were sanded with 400, 600, 800, 1000, and 1200 mesh sandpaper, respectively. Finally, they were etched using a Keller etcher. The microstructural characterization of the experimental samples was carried out after metallographic examinations. For this purpose, following the cold embedding process, the surfaces of the samples taken into bakelite were sanded with 400, 600, 800, 1000, and 1200 mesh sandpapers, respectively. After the sanding process, the surfaces of the experimental samples were polished with 3- μm and 1- μm seals. At the last stage of metallographic studies, after the sanding and polishing operations, the experimental samples were etched using a 5% HF solution. Optical microstructure examinations of the experimental samples were performed at different magnification rates by using a Hardway metallurgical optical microscope (Hardway Hardness Testing Equipments, China), an SU 1510 scanning electron microscope (SEM; Hitachi High-Tech, Japan) was used for the determination of reinforcement element particles that exhibit distribution within the non-reinforcement AA 2014 alloy and the matrix structure, and energy dispersive spectrometry (EDS) analyses were performed with SEM device. For the microhardness measurements of the experimental samples, a Hardway microhardness device (Hardway Hardness Testing Equipments) was used, and

the measurements were performed under a load of HV 0.1. For comparative hardness results, the average hardness values were calculated by taking at least three measurements from each sample. The hardness measurements were carried out at 25°C room temperature.

The surfaces of the non-reinforced AA 2014 aluminum alloy, composite, and hybrid composite materials were polished with a 1- μm diamond solution and cleaned with alcohol. In the block-on-disc wear tests (TurkYus Makina R&D Production Technologies, Turkey), a 10-N load, four different sliding distances (100 m, 200 m, and 400 m), and 0.5- m s^{-1} sliding speed were used. The counter abrasive used in the wear tester was 50 mm in diameter, of 65 HRC hardness, and made of AISI 4140 steel material. After the wear tests, SEM examinations were performed for microstructure analyses of the experimental samples.

RESULTS AND DISCUSSION

In this study, a non-reinforced AA 2014 alloy was used, and composite/hybrid experimental samples were prepared by adding CaSiO_3 and wood ash particle reinforcements in different ratios to the alloy's main matrix structure. Grain sizes and shapes of the matrix and reinforcement particles are important parameters in terms of pressing and sintering attitudes, especially in terms of porosity formation.²⁵ The initial SEM images of the matrix and reinforcement materials used in the study are shown in Fig. 1.

It can be seen from the SEM images of the matrix and reinforcement particles in Fig. 1 that the AA2014 matrix material produced by the gas atomization method is in the form of spherical powder (Fig. 1a), while the reinforcement particle CaSiO_3 has a large-small needle-edged and sharp-edged shape and morphology (Fig. 1b), and the wood ash particles have an irregular shape and morphology. After the sintering, the density changes of the

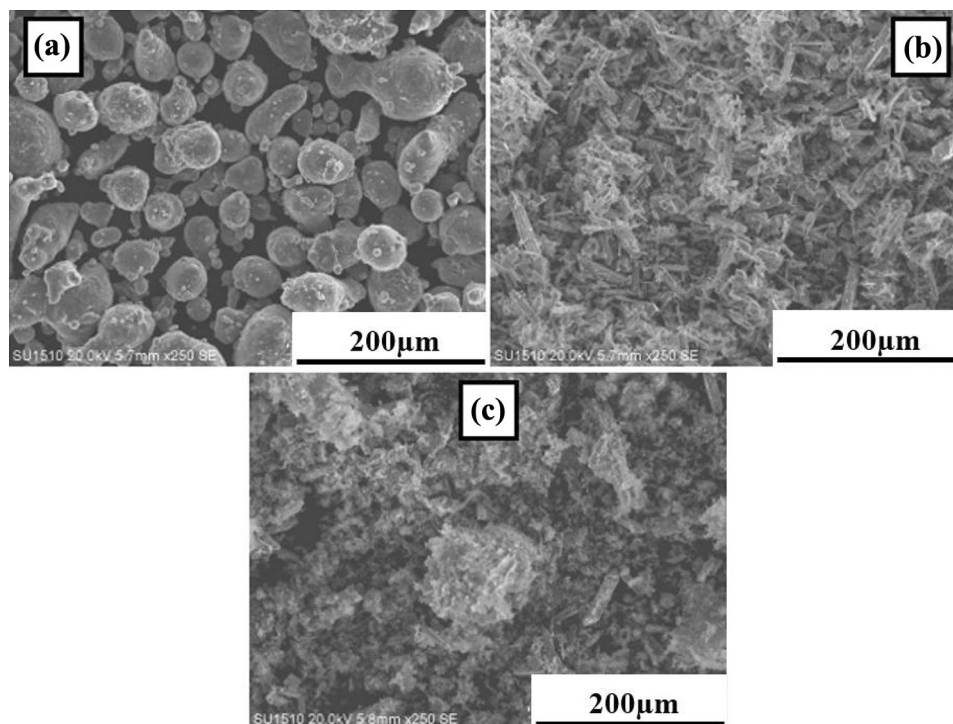


Fig. 1. SEM images of matrix and reinforcement powders: (a) AA2014, (b) CaSiO₃, (c) wood ash.

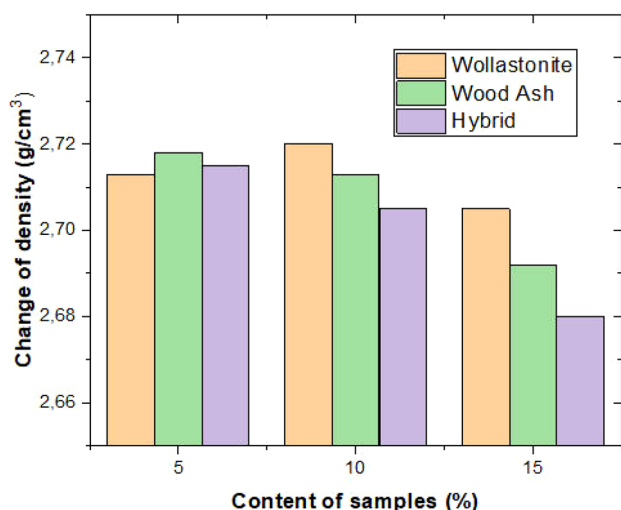


Fig. 2. Density changes for each sample.

non-reinforced AA 2014 aluminum alloy, which is the main matrix structure, and the composite/hybrid experimental samples produced with CaSiO₃ and wood ash solid phase particle reinforcements are shown in Fig. 2.

The Archimedes density value obtained after the sintering process of the AA 2014 aluminum alloy was 2.707 g/cm³. It was determined that the density values of the composite materials produced by reinforcing CaSiO₃ and wood ash (5%, 10%, and 15%) in different proportions into the AA 2014 matrix material increased by a certain amount (Fig. 2). When the produced composite materials

were compared, it was found that, with an Archimedes density value of 2.720 g/cm³, the composite material reinforced with 10% wollastonite was the material that had the highest density. Due to the fact that the particle sizes, density values, and pressability attitudes of the used powders were different, the final densities of each material differed from each other, even if the reinforcement ratios were the same in the composite. It was found that, in the hybrid composite materials, the density value showed an increase of up to a 5% reinforcement rate, while in materials with the 10% and 15% reinforcement rates, the density value decreased. It was observed that, with an Archimedes density value of 2680 g/cm³, the hybrid composite material containing a 15% reinforcement ratio had the lowest density value. In general, it can be stated that the decrease occurring in the density values of the hybrid composite materials compared to the composite materials is due to the gaps observed on the bonding/interface surfaces of the AA 2014 aluminum alloy matrix material and the ceramic particles. It can be said that the amount of gaps observed on the interface increases due to an increase in the amount of particles and the density decrease in parallel with this situation.²⁶ Optical and SEM images obtained after sintering of the non-reinforced AA 2014 aluminum powder metal alloy used as a matrix for the production of composite/hybrid experimental samples are given in Fig. 3a and b. When both optical and SEM microstructure images are examined, it can be stated that the sintering temperature and time (600°C and 1 h) are

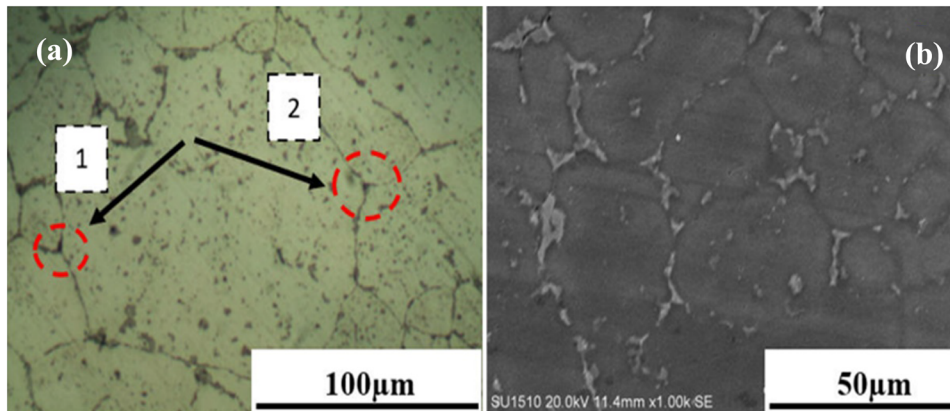


Fig. 3. Optical (a) and SEM images (b) of AA 2014.

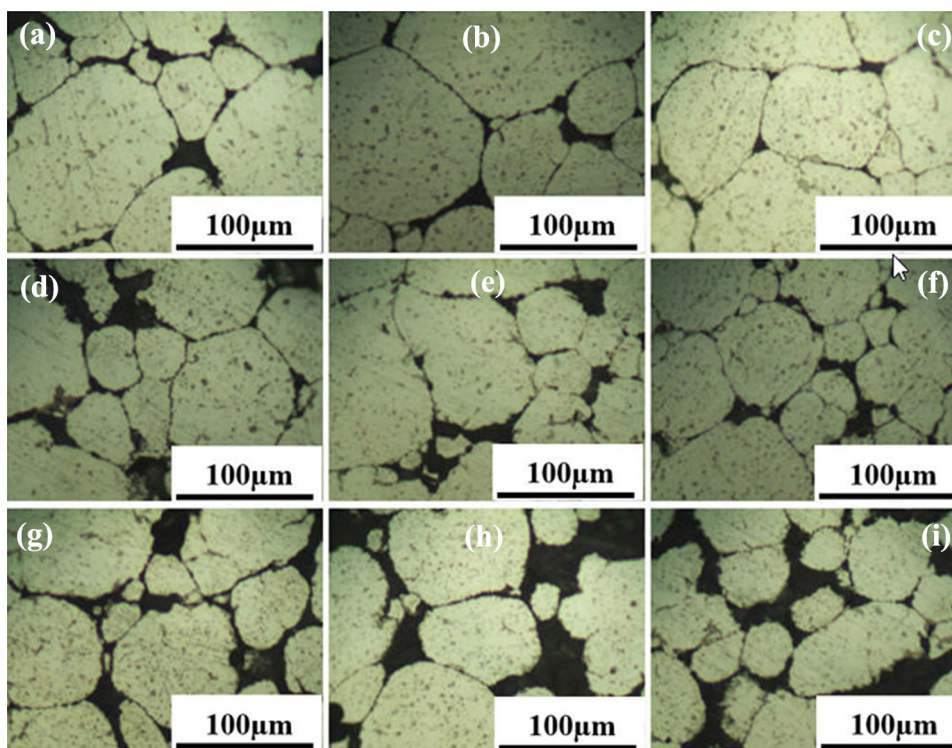


Fig. 4. Optical microscope images of samples: (a) WO5, (b) WO10, (c) WO15, (d) WA5, (e) WA10, (f) WA15, (g) H5, (h) H10, (i) H15.

appropriate in terms of material grain structure and pore formation. In terms of sintering temperature and duration, it can be said that the pores are almost closed and are formed close to a closed and spherical shape, especially at the grain boundaries.²⁷ This situation can be considered as the completion of sintering, especially in terms of grain structure and pore formation. The pore shapes which are mainly spherical or polygonal shapes at the triple-grain junction points (Fig. 3a, 1, 2), which are especially sought after in the sintering process,²⁸ can be interpreted as completing the sintering mechanism for this material.

The optical and SEM microstructures of the composite materials produced in the AA 2014 aluminum metal matrix structure with wollastonite and wood ash powder particle reinforcement after sintering are shown in Figs. 4 and 5, respectively. When the optical microscope images are examined, it can be seen that, after sintering, the pores of the AA2014 aluminum alloy are at the grain boundaries and junction points. It is known that pores remain in the structure after pressing in parts produced by the powder metallurgy method, and some of these pores move into the grain during sintering in terms of a high-temperature resistance mechanism and sintering attitude.²⁹ It can be seen that, with the

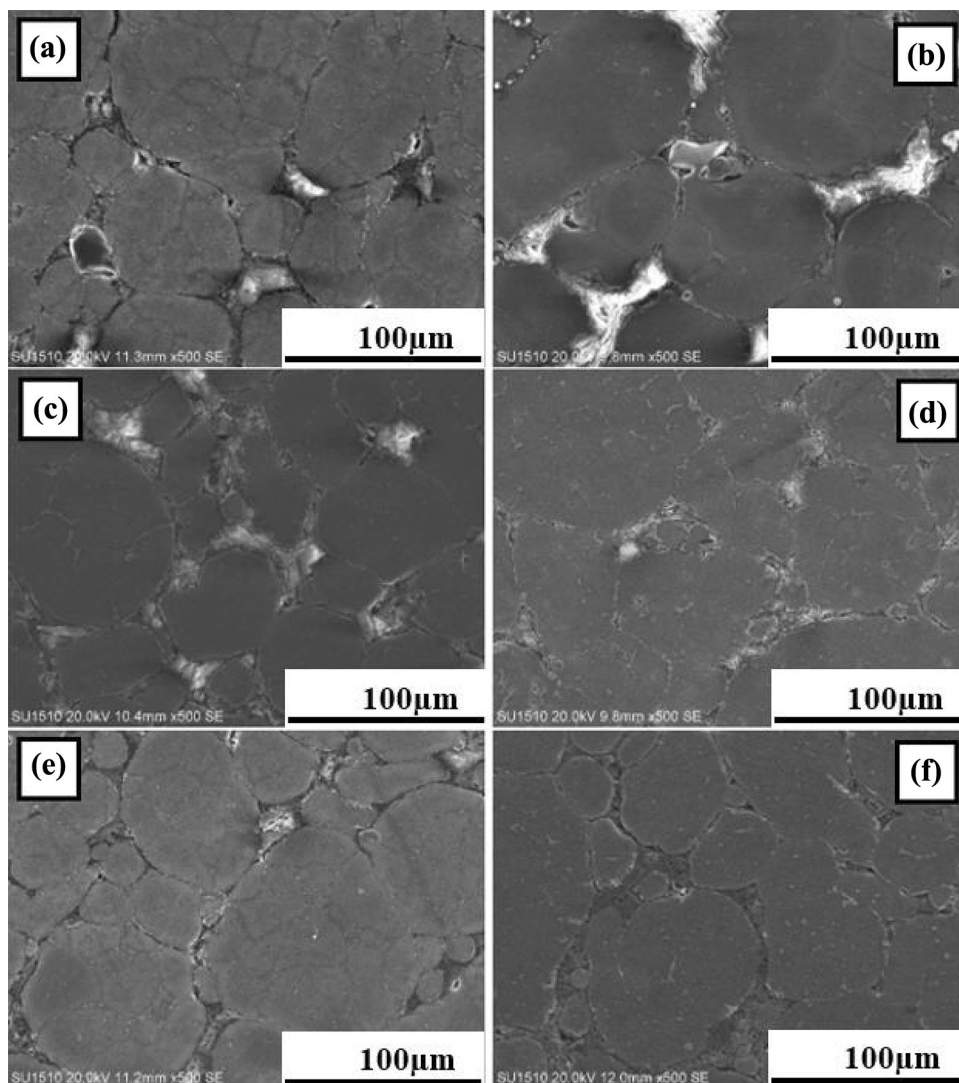


Fig. 5. SEM images of samples: (a) WO5, (b) WO10, (c) WO15, (d) WA5, (e) WA10, (f) WA15.

increase of both wollastonite and wood ash particle reinforcement phases added to the aluminum matrix material, the pores are concentrated at the grain boundary and near the grain boundary (Fig. 4).

The microstructural distribution of the particle reinforcements was revealed more clearly, especially from the SEM images (Fig. 5). When this situation was evaluated in terms of density values in the composite materials, it was observed that there was an increase in the density values of the wollastonite- and wood ash-reinforced composite materials containing 10% reinforcement, as opposed to the formation of pores in the material microstructures, compared to AA 2014 aluminum alloy without reinforcement.

When the SEM images of composite/hybrid materials with the aluminum metal matrix and with wollastonite and wood ash particle reinforcement were examined (Figs. 5 and 6), it was determined that the particle reinforcement geometries and

shapes were mostly distributed at grain boundaries and more clearly compared to the optical microstructure images. Compared to the wollastonite-reinforced composite materials, it can be seen that wood ash exhibits a more suitable distribution in microstructural terms in the wood ash-reinforced composites (Fig. 5).

Considering the sintering process in the powder metal materials and especially the liquid phase sintering mechanism,³⁰ it was determined that wood ash mostly exhibited a homogeneous distribution at the grain boundaries, and a microstructural formation such as the liquid phase sintering mechanism occurred. It can be seen that in both the composite and the hybrid composite materials the particle phases exhibit intense clustering or clumping at the grain boundaries due to the increasing particle reinforcement amounts. When elemental mapping and microstructure images applied to the hybrid composite material produced by these two particle reinforcements were examined (Fig. 7), it

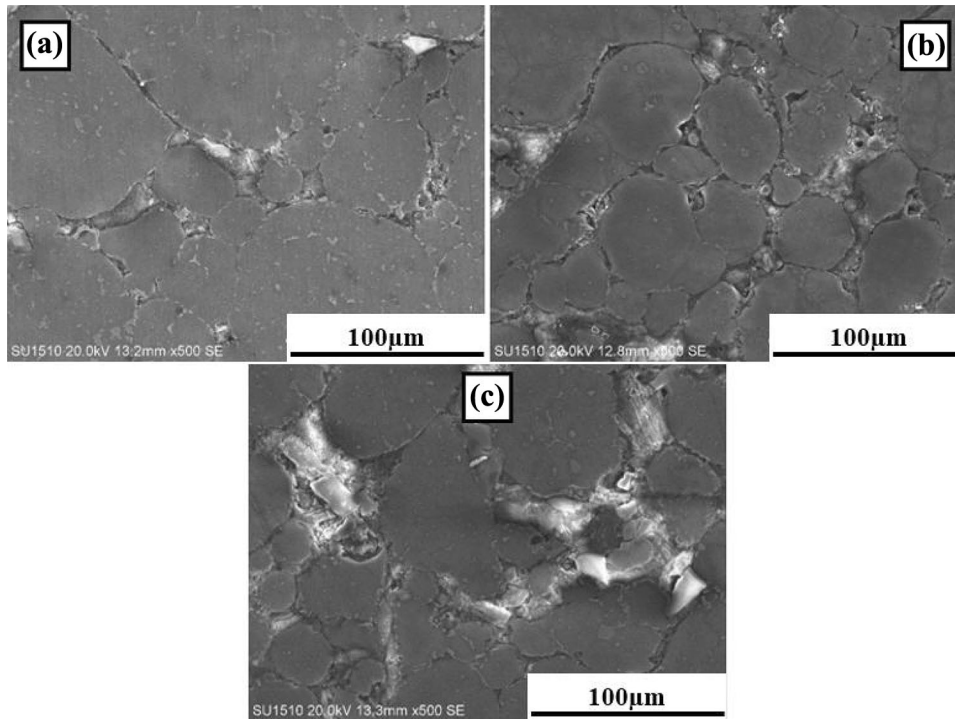


Fig. 6.. SEM images of samples: (a) H5, (b) H10, (c) H15.

was found that the chemical compositions representing the contents of wollastonite and wood ash (Ca, O, K, and Si) were distributed at the grain boundaries.

When the hybrid composite SEM images were examined (Fig. 6), it was determined that the material grain structure and pore relationship were negatively affected, especially in the combination of wollastonite and wood ash. Especially in the hybrid composite materials produced after the application of double reinforcement, it was observed that both wettability and a good interface bond were not shown (Fig. 6c), and in parallel with this situation, the density values also decreased under the increasing particle reinforcement amount.

In order to determine the elemental distribution definitions in the composite and hybrid composite materials, the results of SEM and EDS analysis of the 15%-reinforced hybrid composite material are shown in Fig. 8. The aim of the EDS analysis is to determine the elemental percentages in a hybrid composite material containing a reinforcing element. EDS analyses were carried out in this material in the form of point and regional analyses from two different regions. In the EDS analysis, which is shown as the number 1 region, it was determined that especially the reinforcement particles settle at the grain boundaries and there were elemental distributions such as Fe, Ca, K, Si, and O in accordance with the material's chemical compositions. In addition, when the EDS analysis of point number 2 taken from the material grain structure

was examined, the elemental percentages of Al and Cu chemicals, which define the AA 2014 matrix material, were obtained.

The hardness results of the AA 2014 aluminum alloy and the AA 2014 aluminum matrix composite-hybrid composite materials are shown in Fig. 9. When the hardness results given in the figure were examined, it was seen that, when the AA 2014 aluminum alloy, composite, and hybrid composite materials were compared, an increase in hardness values occurred with an increase in reinforcement particles. Due to the differences in hardness values exhibited by the wollastonite and wood ash reinforcement particles, average hardness values were obtained in the hybrid composite materials. In the composite materials produced with two different reinforcement contents, the wollastonite reinforcement provided a higher hardness increase compared to the wood ash reinforcement. In particular, the fact that the hardness increase is high in the wollastonite-reinforced composite material can be explained by it including hard reinforcement phases such as CaO, SiO₂, Al₂O₃, and Fe₂O₃.³¹ In terms of all the materials, the highest obtained hardness value (70.65 HV) was determined in the composite material with a wollastonite content of 15%. In addition, the highest hardness increase was also calculated as 38.52% in this material. Moreover, this situation can be explained by the fact that hard particles restrict grain boundary and dislocation movements, and that these particles resist plastic deformation under pressure.³²⁻³⁴

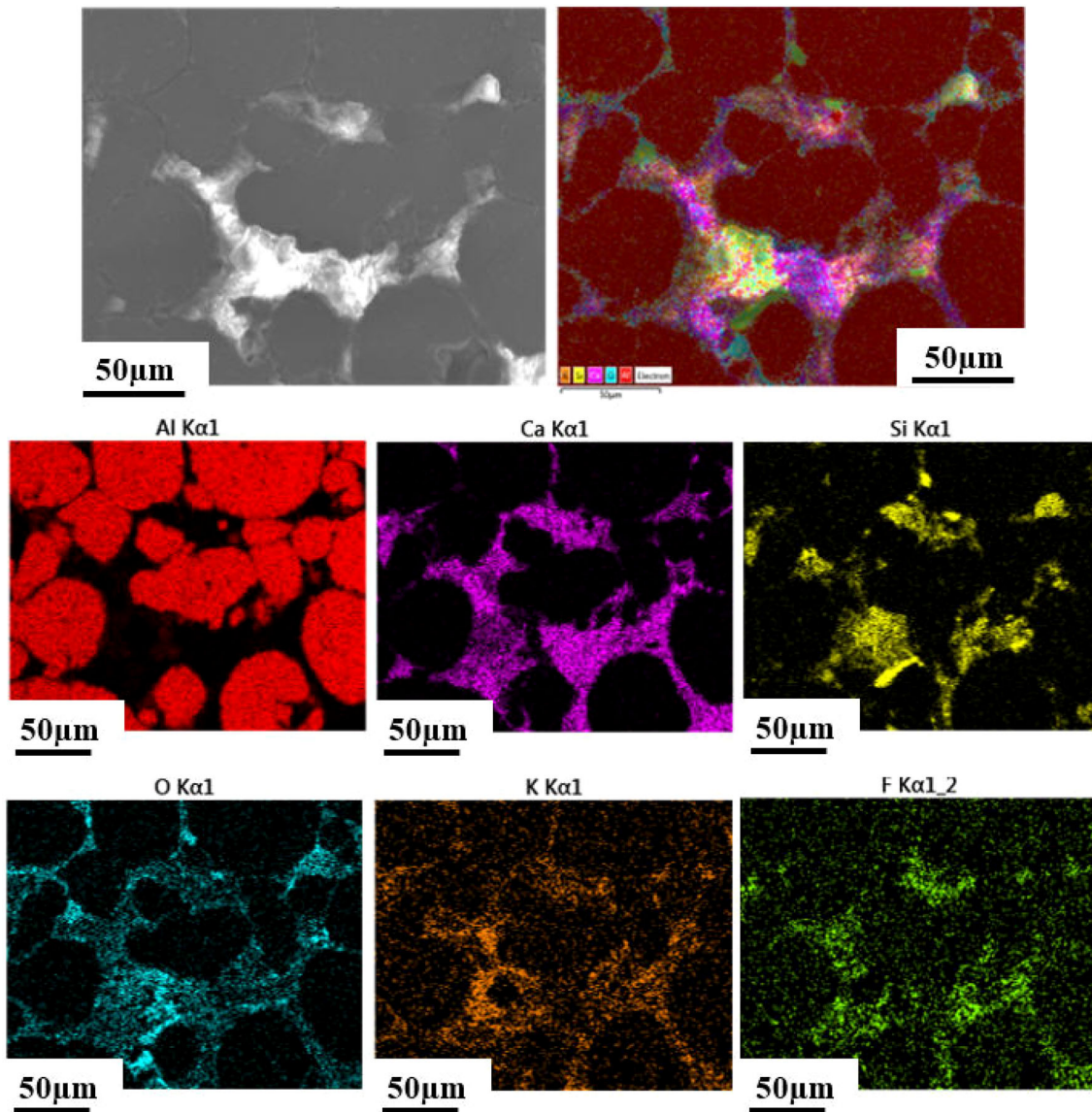


Fig. 7. SEM images and elemental mapping of hybrid (15%) sample.

The weight loss results of the non-reinforced AA 2014 aluminum alloy and composite-hybrid materials with different amounts of reinforcement contents under a 10-N load are shown in Fig. 10. As a result of the applied wear tests, it was observed that particle-reinforced composite materials exhibited wear rates at lower values. The increased content of reinforcement particles led to an increase in hardness, effectiveness at grain boundaries, a decrease in the contact area between the matrix and the opposite surface, and an improvement in wear resistance.³⁵ Thus, it was found that weight losses are reduced in the composite and hybrid composite materials produced with increased reinforcement ratios compared to the matrix aluminum alloy. It is known that the wear behavior and weight losses in materials are affected by factors such as

material grain size, the amount of porosity in the microstructure, and the strength and hardness values.³⁶

During the wear test of the AA 2014 aluminum alloy and the AA 2014 aluminum matrix composite-hybrid composite materials, the wear mechanisms and especially the effects of reinforcement particles on wear behavior were examined. SEM images of the non-reinforced AA 2014 aluminum, the composite containing 15% particle reinforcements, and hybrid composite materials after wear testing under the 10-N load are given in Fig. 11. When the wear surface images are examined, it can be seen that there are debris and groove formations occurring parallel to the sliding direction.^{37,38} It was found that there were debris, crater, and plastic deformation zones on the worn surface of the AA 2014

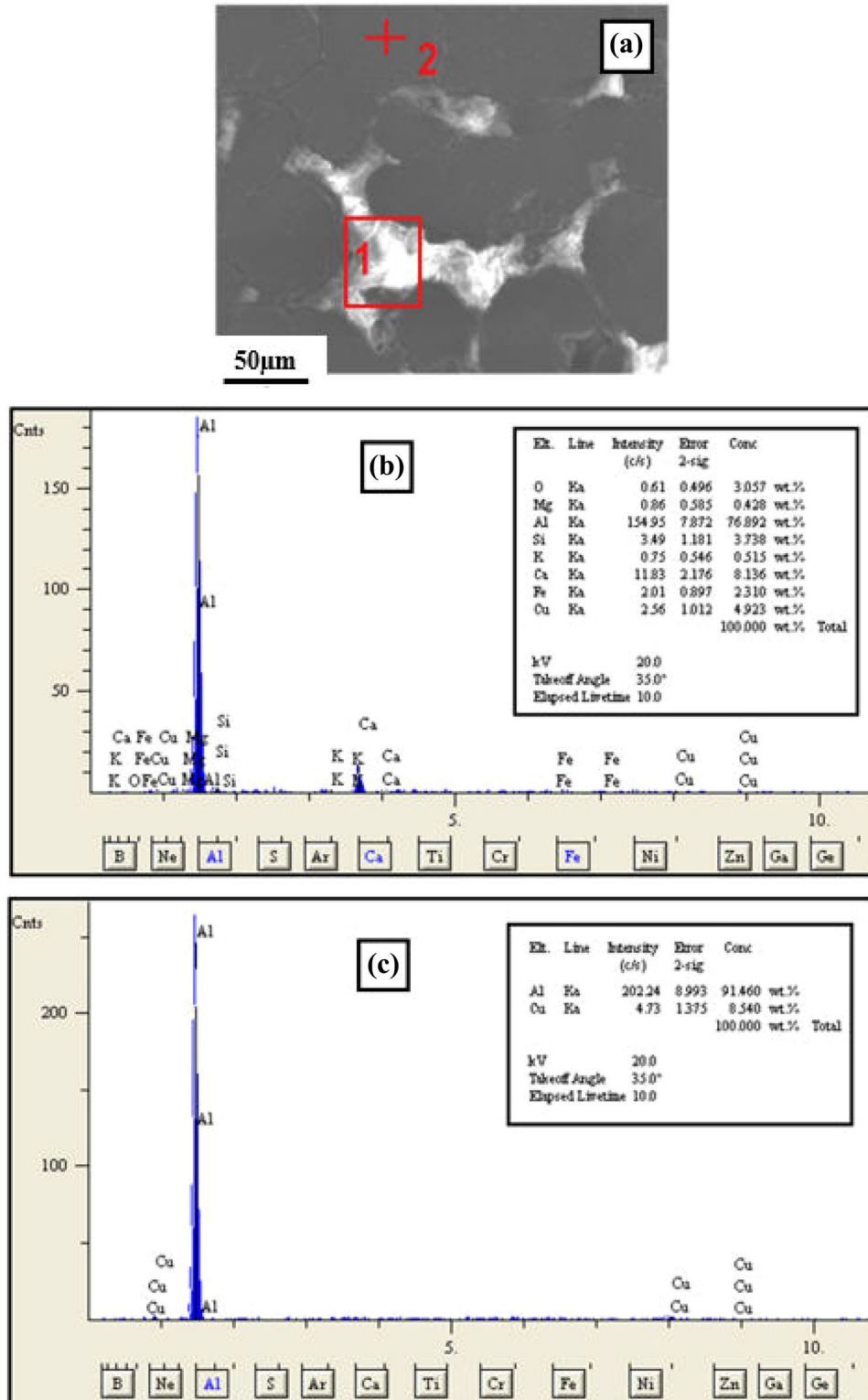


Fig. 8. SEM image (a) and EDS analysis (b, c) of the hybrid (15%) sample.

aluminum alloy which did not contain a reinforcement. Considering this situation, it can be stated that the abrasive wear mechanism is exhibited.^{39,40} It is known that AA 2014 aluminum material, which does not have a waste ceramic particle

reinforcement, is subjected to more deformation than ceramic particle-reinforced materials as a result of wear testing.^{41,42} When the composite and hybrid composite materials with 15% reinforcement rates are examined in Fig. 11, it can be stated

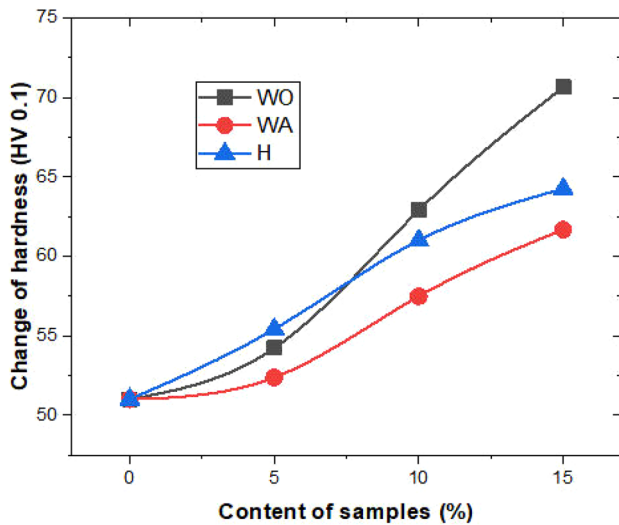


Fig. 9. Micro-hardness test results of samples.

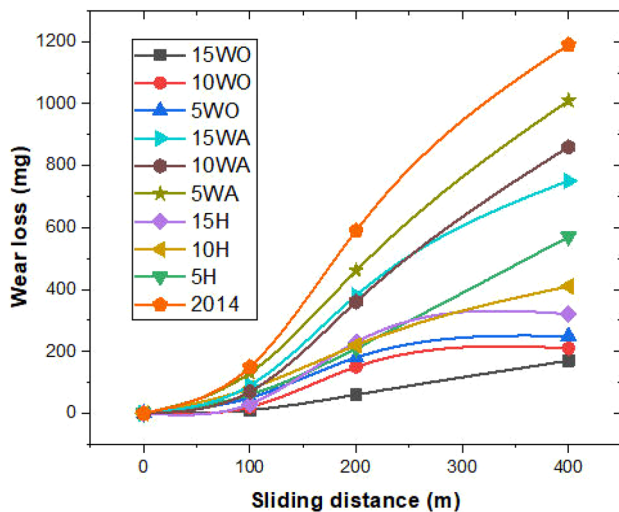


Fig. 10. Wear test results of samples.

that the wollastonite-containing material has low volume losses (Fig. 10) as well as deep grooves and exhibits a better wear behavior compared to the other materials. It can be said that the oxide layers together with the friction heat generated during wear, as well as the oxidized phases contained in the wollastonite content, are effective in the formation of these grooves.

The wood ash used as reinforcement material in the study has no commercial value. Since wood ash is supplied free of charge from factories and ovens that bake bread on wood fires, some costs such as transportation of this material have been ignored. Wollastonite has a unit price just like traditional reinforcements and this is reflected in the price analysis. When Fig. 12 is examined, the production costs of high-cost conventional reinforcement materials (SiC and B₄C) and alternative reinforcement

materials used in this study are compared. For a clear understanding of the unit price analysis, the costs of the highest (15%) reinforced composites were calculated. In the unit price analysis, it can be seen that the highest price belongs to the B₄C-reinforced composites (358 \$/kg). Although the unit price of SiC-reinforced composites (337 \$/kg) is lower than the B₄C-reinforced composites, it is higher than wood ash (328.1 \$/kg) and wollastonite (328.8 \$/kg)-reinforced composite materials.

In addition to the fact that wood ash has no commercial value, it can be used as a supplement in materials that allow mixing in the solid phase, such as AMCs. It also allows a reduction in the raw material cost, which is important for sustainable environmental policies, due to the harmless disposal of this waste generated in bread ovens. Wood ash and wollastonite reinforcing the AA2014 aluminum matrix can improve the mechanical properties of the material such as hardness as well as reducing the production cost. In this context, similar results were obtained in terms of hardness value in our previous study⁴³ with AA2014 matrix reinforced with B₄C and SiC. As a result, this can make waste reinforcement materials attractive and can significantly increase the added value loaded on the waste.

CONCLUSION

AA2014 aluminum alloy, AA2014/wollastonite, AA2014/wood ash, and AA2014/wollastonite/wood ash composite-hybrid materials (5 wt.%, 10 wt.%, and 15 wt.%) were produced using the powder metallurgy method, and the effects of solid waste particles on the microstructure, hardness, and wear behavior were examined. The results obtained can be summarized as follows:

- Low-cost AA2014/solid particle-reinforced composite-hybrid material combinations can be produced by the powder metallurgy method.
- In the production of hybrid composites with high reinforcement amounts of solid particles, acceptable porosity formations and low density can be observed.
- Whereas the lowest amount of porosity was determined in AA 2014 alloy, the highest porosity ratio was determined in the AA2014/wollastonite/wood ash hybrid material with 15% particle reinforcement.
- The addition of solid waste particles increased the hardness and wear resistance. The best hardness and wear behavior were determined in AA2014/15% wollastonite composite material.
- The addition of solid waste particles with ceramic content to the aluminum matrix minimized volume losses while improving the wear resistance of the material.
- It can be recommended that, in addition to traditional ceramic particles, AA2014/solid particle-reinforced composites can be used in applications where wear resistance is desired.

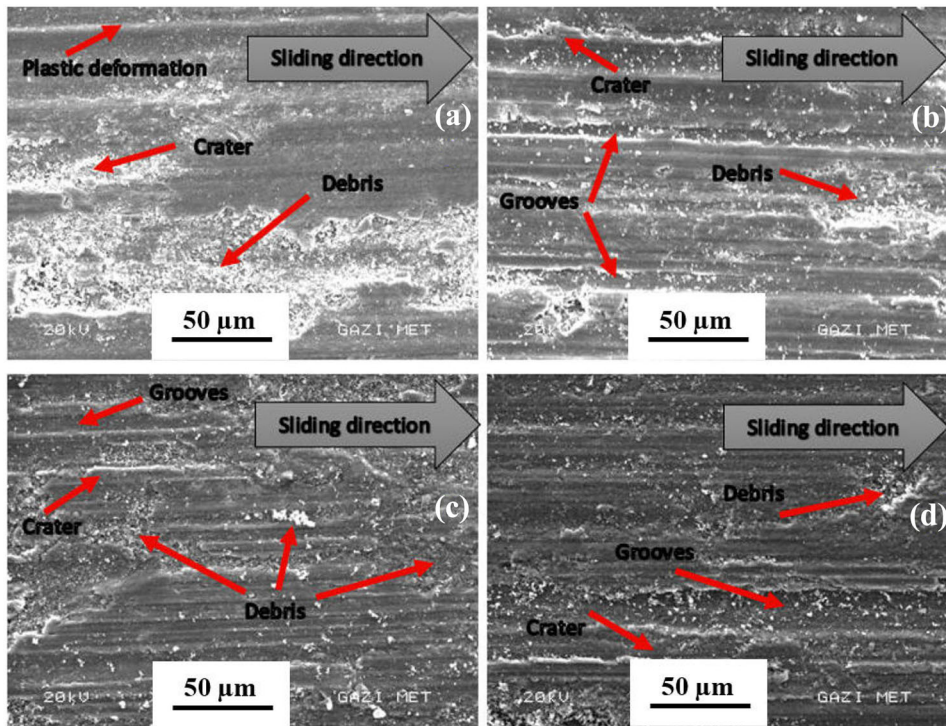


Fig. 11. SEM images of sample worn surfaces: (a) AA 2014 alloy, (b) WA15, (c) H15, (d) WO15.

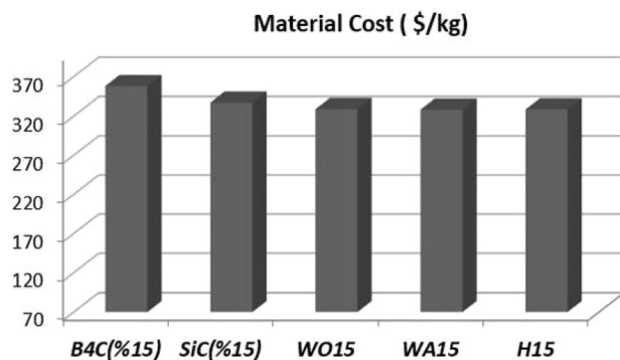


Fig. 12. Cost analysis of materials.

reproduction in any medium or format, as long as you give appropriate credit to the original author(s) and the source, provide a link to the Creative Commons licence, and indicate if changes were made. The images or other third party material in this article are included in the article's Creative Commons licence, unless indicated otherwise in a credit line to the material. If material is not included in the article's Creative Commons licence and your intended use is not permitted by statutory regulation or exceeds the permitted use, you will need to obtain permission directly from the copyright holder. To view a copy of this licence, visit <http://creativecommons.org/licenses/by/4.0/>.

FUNDING

Open access funding provided by the Scientific and Technological Research Council of Türkiye (TÜBİTAK).

CONFLICT OF INTEREST

The authors declared no potential conflicts of interest with respect to the research, authorship, and/or publication of this article.

OPEN ACCESS

This article is licensed under a Creative Commons Attribution 4.0 International License, which permits use, sharing, adaptation, distribution and

REFERENCES

1. J. Jain, A.M. Kar, and A. Upadhyaya, *Mater. Lett.* 58, 2037 (2004).
2. M. Kok, *J. Mater. Process. Technol.* 161, 381 (2005).
3. S.K. Mukherjee and G.S. Upadhyaya, *Trans. JIM* 26, 763 (1985).
4. Y. Sahin and S. Murphy, *J. Mater. Sci.* 31, 5399 (1996).
5. B. Bostan, *J. Fac. Eng. Archit. Gazi Univ.* 23, 343 (2008).
6. H. Gökmeşe, U. Taşçı, and B. Bostan, Experimental investigation of AA2014/SiC composite materials prepared by powder metallurgy method, in *Presented at the 2nd International Conference on Material Science and Technology in Cappadocia 11–13* (2017).
7. P.K. Bardhan, S. Patra, and G. Sutradhar, *Mater. Sci. Appl.* 1, 152 (2010).
8. A. Bahrami, N. Soltani, M.I. Pech-Canul, and C.A. Gutiérrez, *Crit. Rev. Environ. Sci. Technol.* 46, 143 (2016).
9. L. Lancaster, M.H. Lung, and D. Sujan, *World Acad. Sci. Eng. Technol.* 73, 1136 (2013).

10. H.S.M. Khierallah, S.M. Bader, K.M. Ibrahim, and I.J. Al-Jboory, *Date Palm Genetic Resources and Utilization* (Springer, Dordrecht, 2015), pp. 97–152.
11. B. Parveez, M.A. Maleque, and N.A. Jamal, *J. Mater. Sci.* 56, 16195 (2021).
12. K.K. Alaneme, T.M. Adewale, and P.A. Olubambi, *J. Mater. Res. Technol.* 3, 9 (2014).
13. B.Q. Ochieze, C.C. Nwobi-Okoye, and P.N. Atamuo, *Def. Technol.* 14, 77 (2018).
14. F.A. Al-Sulaiman, *Appl. Compos. Mater.* 9, 369 (2002).
15. N. Soltani, A. Bahrami, M.I. Pech-Canul, and L.A. González, *Chem. Eng. J.* 264, 899 (2015).
16. Ch. Hima-Gireesh, K.G. Durga-Prasad, K. Ramji, and P.V. Vinay, *Mater. Today Proc.* 5, 3289 (2018).
17. A.A. Abdulrazaq, S.R. Ahmed, and F.M. Mahdi, *Clean. Eng. Technol.* 11, 100565 (2022).
18. M.R. Hossain, M.H. Ali, M.A. Amin, M.G. Kibria, and M.S. Ferdous, *Int. J. Eng. Mater. Manuf.* 2, 94 (2017).
19. D.S. Prasad and A.R. Krishna, *J. Mater. Sci. Technol.* 28, 367 (2012).
20. V.R. Subrahmanyam, J. Madhukiran, G. Naresh, and S. Madhusudhan, *Int. J. Adv. Sci. Technol.* 94, 49 (2016).
21. M. Satheesh and M. Pugazhivadivu, *Physica B Condens. Matter* 572, 70 (2019).
22. S. Balasubramani, B. Natarajan, B. Kaliyaperumal, and S.J.S. Chelladurai, *Overseas Foundry China Foundry* 15, 449 (2018).
23. S.R. Rallabandi and R.G. Srinivasa, *J. Inst. Eng. India Ser. C* 100, 13 (2019).
24. P. Lakshmikanthan and D.B. Prabu, *J. Balk. Tribol. Assoc.* 2, 4008 (2016).
25. Y.I. Kim, W. Lee, J.M. Jang, S.W. Ui, and G.S. An, *J. Alloys Compd.* 747, 211 (2018).
26. G. Manohar, K.M. Pandey, and S.R. Maity, *Mater. Today Proc.* 38, 2157 (2021).
27. T. Wang, L. Yang, Z. Tang, C. Liu, Y. Ma, L. Wu, H. Yan, Z. Yu, and W. Liu, *Mater. Sci. Eng. A* 822, 141606 (2021).
28. Ö. Özgün and H. Gülsoy, *Turk. J. Nat. Sci.* 9, 6 (2020).
29. T.I.A.N. Wenming, L.I. Songmei, L.I.U. Jianhua, Y.U. Mei, and D.U. Yujie, *Chin. J. Aeronaut.* 30, 1777 (2017).
30. R.M. German, P. Suri, and S.J. Park, *J. Mater. Sci.* 44, 1 (2009).
31. S.P. Dwivedi, R. Sahu, A. Saxena, V.K. Dwivedi, K. Srinivas, and S. Sharma, *Proc. Inst. Mech. Eng. Part E J. Process Mech. Eng.* 236, 160 (2022).
32. D.S. Prasad, C. Shoba, and N. Ramanaiah, *J. Mater. Res. Technol.* 3, 79 (2014).
33. M. Triwikantoro, M. Zainuri, R. Bäßler, and Darminto, *J. Phys. Sci.* 30, 81 (2019).
34. F. Aydın, *J. Mater. Eng. Perform.* 30, 8560 (2021).
35. S. Demirdal and F. Aydın, *Mater. Chem. Phys.* 277, 125520 (2022).
36. U. Tasci, T.A. Yilmaz, and B. Bostan, *Tribol. Int.* 180, 108231 (2023).
37. V. Kaushik, A. Aherwar, A. Sharma, S. Kumar, S. Aftab, R. Khargotra, and T. Singh, *Results Eng.* 19, 101311 (2023).
38. H. Gökmeşe, H.B. Karadağ, and H. Taşdöğen, *Trans. Indian Inst. Met.* 75, 435 (2022).
39. M. Yıldırım and D. Özyürek, *High Temp. Mater. Process.* 37, 619 (2018).
40. M. Yıldırım, D. Özyürek, and M. Gürü, *Arab. J. Sci. Eng.* 41, 4273 (2016).
41. M.K. Chaanthini, M. Govindaraju, and S. Arul, *J. Inst. Eng. India Ser. D* 101, 265 (2020).
42. K. Sekar and P. Vasanthakumar, *Mater. Sci. Forum* 1081, 11 (2023).
43. H. Gökmeşe and H.B. Karadağ, *Gazi Univ. J. Sci. Part C Des. Technol.* 6, 385 (2018).

Publisher's Note Springer Nature remains neutral with regard to jurisdictional claims in published maps and institutional affiliations.